Multilayer graphene with a superlattice potential

Sayed Ali Akbar Ghorashi and Jennifer Cano

Phys. Rev. B **107**, 195423 — Published 12 May 2023

DOI: 10.1103/PhysRevB.107.195423

Multilayer graphene with a superlattice potential

Sayed Ali Akbar Ghorashi[1]* and Jennifer Cano[1,2]
[1] *Department of Physics and Astronomy, Stony Brook University, Stony Brook, New York 11974, USA and*
[2] *Center for Computational Quantum Physics, Flatiron Institute, New York, New York 10010, USA*
(Dated: April 24, 2023)

Bernal stacked bilayer graphene subject to a superlattice potential can realize topological and stacked flat bands [arXiv:2206.13501]. In the present work, we extend the study of a superlattice potential on graphene heterostructures to trilayer and quadrilayer graphene. Comparing Bernal- and chirally-stacked multilayers reveals that the latter are more suitable for realizing stacks of many flat bands. On the other hand, Bernal-stacked graphene heterostructures can realize topological flat bands. Imposing two simultaneous superlattice potentials enhances the viability of both regimes.

I. INTRODUCTION

Twisted heterostructures have recently emerged as a highly tunable family of materials exhibiting a remarkable range of phenomena and showing promise as a quantum simulation platform for strongly correlated and topological physics [1–14]. The most prominent example is twisted bilayer graphene (TBLG), which can host strongly correlated insulating phases and superconductivity [2, 9]. Subsequent studies on twisted multilayer graphene heterostructures also exhibit correlation-driven physics [15–24]. Twisted bilayers beyond graphene have further demonstrated the versatility and tunability of these platforms [10, 12, 13, 25–43].

Despite the excitement and rapid progress, twisted heterostructures also suffer from new types of disorder, such as inhomogenous angle and strain, lattice relaxation, and sensitivity to the substrate. Together these factors severely impact sample reproducibility [44]. Hence, alternative approaches to realize flat bands and moiré physics is desirable.

Conceptually, twisting adjacent layers induces a spatially modulated interlayer coupling that quenches the kinetic energy, resulting in flat bands and interaction-dominated physics. We propose a change of paradigm where interlayer modulation is replaced by intralayer modulation, in the form of a superlattice potential.

A spatially modulated superlattice potential can be achieved by inserting a patterned dielectric between the gate and the sample. This set-up that has been realized experimentally [45–47] and studied theoretically [48–55] in monolayer graphene. The effect of a superlattice potential on bilayer graphene (BLG) has also been studied [56–58]. While the original works did not consider flat band physics, we recently revisited BLG with a superlattice potential and showed that under experimentally feasible conditions, two distinct regimes of flat bands can be achieved [59]: the first regime exhibits topological flat bands with non-zero valley Chern number, C. The second regime, dubbed the "stack of flat bands," exhibits many flat bands, spanning a large portion of the relevant energy spectrum, but with vanishing valley Chern number. Superlattice potentials applied to other systems can also promote correlation-driven physics [60–63].

In the present work, we ask under what conditions the two distinct regimes can be realized in multilayer graphene with a superlattice potential. In particular, we studied a superlattice potential on trilayer graphene (TLG) and quadrilayer graphene (QLG) for both the case of chiral (ABC, ABCA) and Bernal (ABA, ABAB) stacked structures. We find that chirally stacked multilayers favor the stacked flat band phase for large superlattice period L, but topological bands can be realized for smaller L. On the other hand, Bernal TLG and QLG are more suitable for topological flat bands, although the latter requires fine-tuning unless an additional sublattice mass is included. In all cases, unlike in BLG, the remote hopping terms cannot be neglected.

The superlattice potential becomes less effective as more graphene layers are added due to screening. This motivates us to consider a second set-up where multilayer graphene is sandwiched between two superlattice gates. In this case, chiral stacked multilayers can realize both flat band regimes.

II. CHIRAL STACKING

We start by discussing chirally stacked multilayer graphene where the the A sites of the upper layer are above the B sites of the lower layer and coupled by the nearest neighbor interlayer hopping amplitude, as shown in Fig. 2(a). In the following we focus on two examples, ABC-stacked TLG and ABCA-stacked QLG to elucidate the effect of a superlattice potential on chirally stacked multilayer graphene.

A. ABC

We start with the brief review of ABC-stacked trilayer graphene in the absence of a superlattice potential. In the basis $(A_1, B_1, A_2, B_2, A_3, B_3)$, a low-energy Hamiltonian

* sayedaliakbar.ghorashi@stonybrook.edu

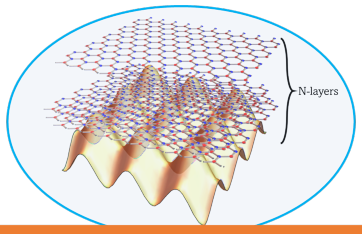

Stacking	Bernal+ bias + sublattice mass		Chiral+ bias	
Flat band regime	Topological	Stacked	Topological	Stacked
Small-medium L (e.g., 10-40 nm)	✓	✘	✓	✓
Large L (e.g., L>40 nm)	✓	✘	✘	✓

FIG. 1. Summary of results. Biased chirally stacked multilayer graphene favors stacked flat bands in the large L regime, but can realize topological flat bands for smaller L. Bernal stacked multilayer graphene realizes topological flat bands as long as a sublattice mass is present.

can be written as [64]

$$H_{ABC}(\mathbf{k}) = \begin{pmatrix} 0 & v\pi^\dagger & 0 & v_3\pi & 0 & \gamma_2/2 \\ v\pi & 0 & \gamma_1 & 0 & 0 & 0 \\ 0 & \gamma_1 & 0 & v\pi^\dagger & 0 & v_3\pi \\ v_3\pi^\dagger & 0 & v\pi & 0 & \gamma_1 & 0 \\ 0 & 0 & 0 & \gamma_1 & 0 & v\pi^\dagger \\ \gamma_2/2 & 0 & v_3\pi^\dagger & 0 & v\pi & 0 \end{pmatrix}, \quad (1)$$

where $\pi = \chi k_x + ik_y$, $\chi = +(-)$ for valley $K(K')$, $v = (\sqrt{3}/2)a\gamma_0/\hbar$ denotes the Fermi velocity of each graphene layer, γ_2 parameterizes intrasublattice hopping between the top and bottom layers, and $v_3 = (\sqrt{3}/2)a\gamma_3/\hbar$ accounts for trigonal warping.

Fig. 2 shows the band structure of (1) with and without the remote hoppings $\gamma_{2,3}$, which are depicted in Fig. 2(a). In the absence of remote hoppings, i.e. $\gamma_{2,3} = 0$, the low-energy bands have a cubic dispersion, as shown in Fig. 2(b). The addition of $\gamma_{2,3} \neq 0$ splits the cubic Dirac fermion into three linearly dispersing cones, as shown in Figs. 2(c)-(e). The remote hoppings are relevant within around $10 - 20$ meV of the charge neutrality point. In contrast, the analogous terms in bilayer graphene are only important within a few meV of the Dirac point [65].

The effect of a displacement field is included via

$$H_{V_0} = \begin{pmatrix} V_0\mathbb{I}_2 & \mathbf{0}_2 & \mathbf{0}_2 \\ \mathbf{0}_2 & \mathbf{0}_2 & \mathbf{0}_2 \\ \mathbf{0}_2 & \mathbf{0}_2 & -V_0\mathbb{I}_2 \end{pmatrix}, \quad (2)$$

which breaks inversion symmetry and opens up a gap in chirally stacked multilayer graphene.

We now consider the effect of a spatially modulated superlattice potential, described by

$$H_{SL}(\mathbf{r}) = \frac{V_{SL}}{2} \begin{pmatrix} \mathbb{I}_2 & \mathbf{0}_2 & \mathbf{0}_2 \\ \mathbf{0}_2 & \alpha\mathbb{I}_2 & \mathbf{0}_2 \\ \mathbf{0}_2 & \mathbf{0}_2 & \beta\mathbb{I}_2 \end{pmatrix} \sum_n \cos(\mathbf{Q}_n \cdot \mathbf{r}), \quad (3)$$

where V_{SL} is the strength of the superlattice potential and the set of $\mathbf{Q}_n$ are its wave vectors. We specialize to the case of a triangular superlattice potential with $\mathbf{Q}_n = Q(\cos(2n\pi/6), \sin(2n\pi/6))$, $n = 1, \ldots, 6$ and $Q = 4\pi/\sqrt{3}L$, which define the "mini Brillion zone" (mBZ) by $\Gamma_m = (0, 0)$, $M_m = \frac{1}{2}\mathbf{Q}_0$, and $K_m = \frac{1}{3}(\mathbf{Q}_0 + \mathbf{Q}_1)$. Note that Γ_m corresponds to the original K point of TLG. The parameters $0 \leq \alpha, \beta < 1$ are the ratio of the superlattice potential felt on one layer relative to the other; the asymmetry between the layers results from the experimental set-up where the superlattice potential is applied only on one side of the multilayer graphene. In the following, we use $\alpha = 0.3$ and $\beta = 0.1$ for both stackings of TLG [66].

Fig. 3 shows the evolution of the band structure of TLG in the triangular superlattice potential versus V_{SL} and V_0, without (first column) and with (second column) remote hoppings. We took the superlattice period to be $L = 50$ nm for comparison to our previous results on BLG [59]; however, a smaller value of L realizes more isolated flat bands, which are less vulnerable to disorder, as we will shortly discuss.

Fig. 3 shows similarities and differences compared to BLG [59]. First, in BLG, isolated topological flat bands appeared in the limit of small V_0 and V_{SL}; we do not observe such bands in chiral TLG. In the opposite limit where the fields are turned up, a regime of many stacked flat bands appears in both BLG and TLG. In TLG, this regime appears at smaller field strength due to the larger density of states near the charge neutrality point.

We further observe that the remote hoppings cause the flat bands to develop a dispersion (Fig. 3(e)) compared to the case without remote hopping (Fig. 3(b)). As the fields are increased, stacked flat bands form with and without remote hopping (Figs. 3(c,f)).

B. ABCA

ABCA-stacked QLG is a chiral multilayer graphene structure with four layers, as shown in Fig. 4(a). It can be described by the following Hamiltonian [64]

$$H_{ABCA}(\mathbf{k}) = \begin{pmatrix} H_{\mathbf{G}} & \Gamma_1 & \Gamma_2 & \mathbf{0}_2 \\ \Gamma_1^\dagger & H_{\mathbf{G}} & \Gamma_1 & \Gamma_2 \\ \Gamma_2^\dagger & \Gamma_1^\dagger & H_{\mathbf{G}} & \Gamma_1 \\ \mathbf{0}_2 & \Gamma_2^\dagger & \Gamma_1^\dagger & H_{\mathbf{G}} \end{pmatrix}, \quad (4)$$

where $H_{\mathbf{G}}$ is the Dirac cone Hamiltonian in each layer and the interlayer couplings $\Gamma_{1,2}$ are given by

$$\Gamma_1 = \begin{pmatrix} 0 & v_3\pi^\dagger \\ \gamma_1 & 0 \end{pmatrix}, \quad \Gamma_2 = \begin{pmatrix} 0 & \gamma_2/2 \\ 0 & 0 \end{pmatrix} \quad (5)$$

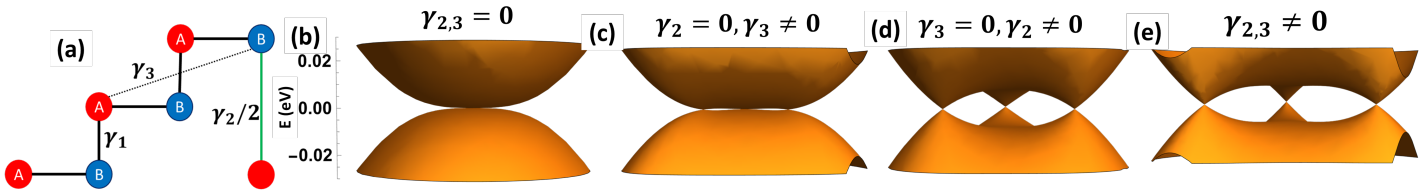

FIG. 2. (a) Schematic of hopping processes in our model of ABC-stacked TLG. (b-e) Band structures of ABC stacked TLG for different values of remote hoppings. We used $\gamma_1 = 0.4$, $\gamma_2 = -0.02$, $\gamma_3 = 0.308$ eV.

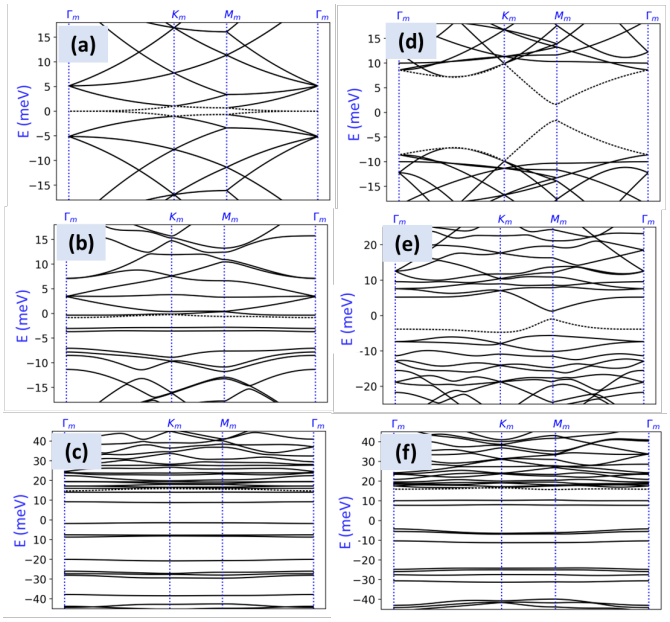

FIG. 3. Band structures of ABC-stacked TLG with a triangular superlattice potential, without (a-c) and with (d-f) remote hoppings. (a,d) $V_{SL} = 0$, $V_0 = 0$ meV, (b,e) $V_{SL} = 5$, $V_0 = 0$ meV, (c,f) $V_{SL} = 20$, $V_0 = -20$ meV. While the low-energy band structure for zero or weak V_{SL} appears gapped in the presence of the remote hoppings (d,e), there are gapless points off the high-symmetry plotted path, consistent with Fig. 2.

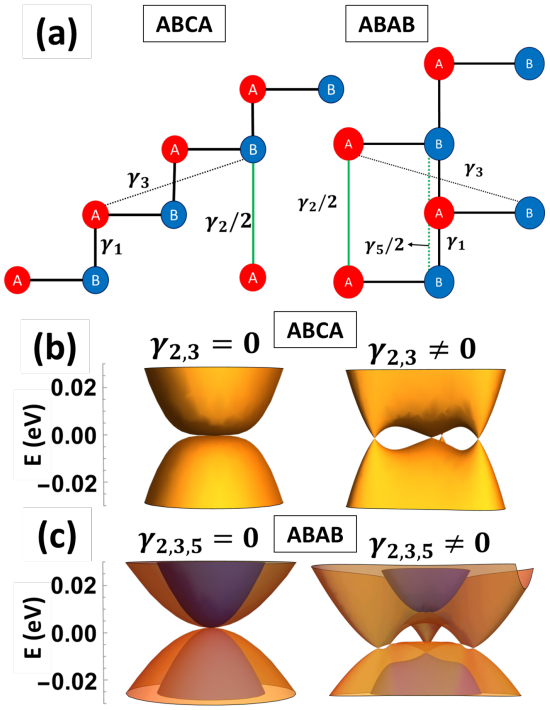

FIG. 4. (a) Schematic representation of the hopping processes included in our model for ABCA and ABAB stacked QLG. Band structure of (b) ABCA-stacked and (c) ABAB stacked QLG with and without the remote hoppings. $\gamma_1 = 0.4$, $\gamma_2 = -0.02$, $\gamma_3 = 0.308$, $\gamma_5 = 0.04$ eV.

Similar to TLG, we define the displacement field and superlattice potentials by

$$H_{V_0} = V_0 \begin{pmatrix} \mathbb{I}_2 & \mathbf{0}_2 & \mathbf{0}_2 & \mathbf{0}_2 \\ \mathbf{0}_2 & \mathbf{0}_2 & \mathbf{0}_2 & \mathbf{0}_2 \\ \mathbf{0}_2 & \mathbf{0}_2 & \mathbf{0}_2 & \mathbf{0}_2 \\ \mathbf{0}_2 & \mathbf{0}_2 & \mathbf{0}_2 & -\mathbb{I}_2 \end{pmatrix} \tag{6}$$

and

$$H_{SL}(\mathbf{r}) = \frac{V_{SL}}{2} \begin{pmatrix} \mathbb{I}_2 & \mathbf{0}_2 & \mathbf{0}_2 & \mathbf{0}_2 \\ \mathbf{0}_2 & \alpha\mathbb{I}_2 & \mathbf{0}_2 & \mathbf{0}_2 \\ \mathbf{0}_2 & \mathbf{0}_2 & \beta\mathbb{I}_2 & \mathbf{0}_2 \\ \mathbf{0}_2 & \mathbf{0}_2 & \mathbf{0}_2 & \eta\mathbb{I}_2 \end{pmatrix} \sum_n \cos(\mathbf{Q}_n \cdot \mathbf{r}), \tag{7}$$

where we use $\alpha = 0.3$, $\beta = 0.1$, $\eta = 0$ throughout this work [66]. In the absence of remote hoppings the low-energy bands have a quartic dispersion. The remote hoppings split the quartic band touching point into the four linearly dispersing cones, shown in Fig. 4(b).

Fig. 5 shows band structures of ABCA QLG in a superlattice potential. Similar to chiral TLG, for small fields, the bands near charge neutrality flatten but do not become isolated. As the fields are turned up, the stacked flat band regime appears; comparing QLG, TLG and BLG, we observed a trend that for more layers of graphene, the stacked flat band regime appears for smaller fields, due to the larger density of states near the charge neutrality point. Comparing Figs. 5(c,f) to Figs. 3(c,f), the remote hopping terms have a more pronounced effect for QLG than for TLG, causing the flat bands to clump together.

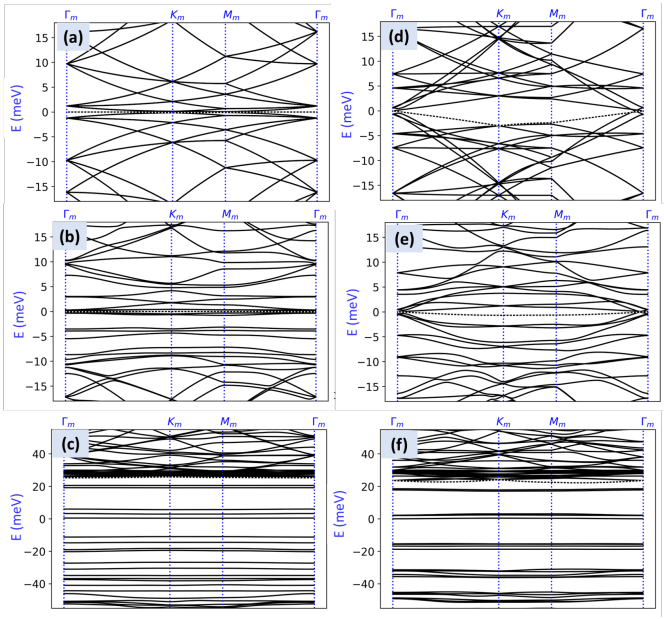

FIG. 5. The band structures of ABCA-stacked QLG without (a-c) and with (d-f) remote hoppings. (a,d) $V_{SL} = 0$, $V_0 = 0$ meV, (b,e) $V_{SL} = 5$, $V_0 = 0$ meV, (c,f) $V_{SL} = 20$, $V_0 = -30$ meV.

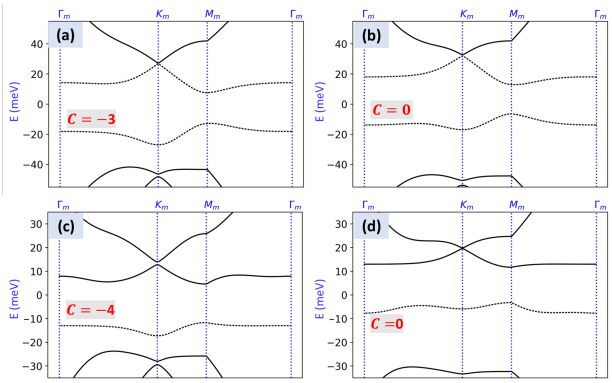

FIG. 6. Chiral multilayer structures with a small superlattice period $L = 15$ nm exhibit gate-tunable topology. Chiral TLG with $V_{SL} = 25$ meV and (a) $V_0 = 15$ meV vs (b) $V_0 = -15$ meV. Chiral QLG with $V_{SL} = 20$ meV and (a) $V_0 = 13$ meV vs (b) $V_0 = -13$ meV.

C. Significance of L

So far, we have fixed the superlattice periodicity at $L = 50$ nm for comparison to Ref. 59. However, a smaller value of L is important to achieve isolated flat bands in multilayer graphene, as we now explain. For multilayer graphene structures, as the number of layers increases, the low-energy density of states also increases. In the presence of a superlattice potential, the increased density of states decreases the inter-band spacing, making the topological indices of individual bands sensitive to small parameter changes. Further, closely spaced bands will

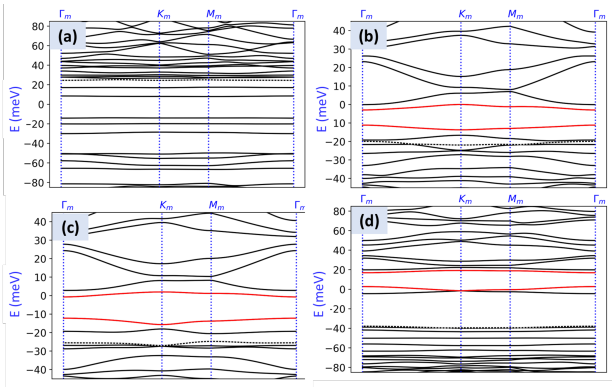

FIG. 7. For a mid-range superlattice periodicity of $L = 35$ nm, changing the sign of V_0 in chiral TLG changes the spectrum from (a) a stacked flat band regime to (b) one with topological flat bands. As V_0 is turned further positive, the stacked band regime does not appear until nearly $V_0 = 80$ meV; the evolution is shown in (c,d). Chiral TLG with $V_{SL} = 40$ meV and (a) $V_0 = -35$ meV, (b) $V_0 = 35$ meV, (c) $V_0 = 45$ meV and (d) $V_0 = 80$ meV. Red indicates topological Chern bands.

be difficult to resolve experimentally in the presence of disorder. Thus, as the number of layers is increased, a smaller value of L is preferred to achieve isolated flat bands.

The minimum value of L achieved by an artificially imposed superlattice is 16nm [47]. At this small value of L, topological flat bands can be realized, as we show in Fig. 6 for $L = 15$ nm. Our results are consistent with those of Ref. 67 and 68, where the superlattice potential is realized by a stacked moiré heterostructure made from slightly misaligned hexagonal boron nitride on TLG. This regime has the additional feature that the topology of the lowest valence band can be altered by changing the sign of V_0.

For mid-range L, the sign of V_0 can tune between the topological and stacked flat band regimes. Fig. 7 shows such an example, where varying V_0 from negative (Fig. 7(a)) to positive (Fig. 7(b)) causes a transition between stacked and topological flat bands when $L = 35$ nm. This occurs because the stacked flat band regime requires a stronger field for positive values of V_0, as shown in Figs. 7(c,d).

III. BERNAL STACKING GRAPHENE

We now turn to studying the effect of a superlattice potential on Bernal-stacked multilayer graphene, specifically ABA TLG and ABAB QLG for three and four layers, respectively.

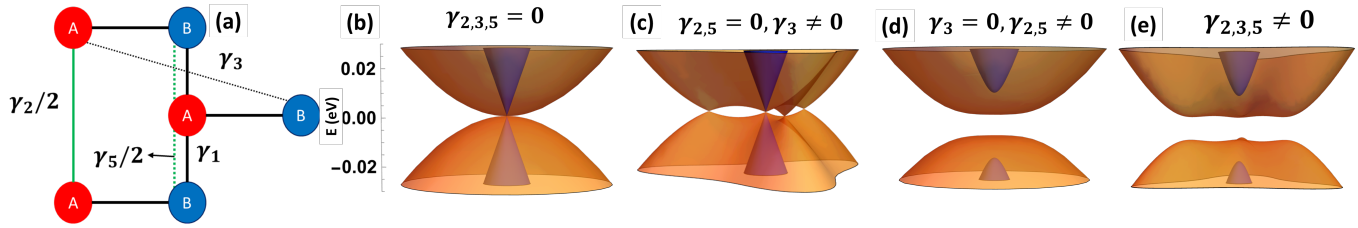

FIG. 8. (a) Schematic representation of the hopping processes included in our model for ABA-stacked TLG. (b-e) band structures of ABA stacked TLG for various configuration of remote hoppings. $\gamma_1 = 0.4$, $\gamma_2 = -0.02$, $\gamma_3 = 0.308$, $\gamma_5 = 0.04$ eV

A. ABA

ABA-stacked TLG is shown in Fig. 8(a). Its Hamiltonian can be written as follows,

$$H_{ABA}(\mathbf{k}) = \begin{pmatrix} 0 & v\pi^\dagger & 0 & v_3\pi & \gamma_2/2 & 0 \\ v\pi & 0 & \gamma_1 & 0 & 0 & \gamma_5/2 \\ 0 & \gamma_1 & 0 & v\pi^\dagger & 0 & \gamma_1 \\ v_3\pi^\dagger & 0 & v\pi & 0 & v_3\pi^\dagger & 0 \\ \gamma_2/2 & 0 & 0 & v_3\pi & 0 & v\pi^\dagger \\ 0 & \gamma_5/2 & \gamma_1 & 0 & v\pi & 0 \end{pmatrix} \tag{8}$$

In ABA-stacked TLG the AA (γ_2, solid green bond in Fig. 8(a)) and BB (γ_5, dotted green bond in Fig. 8(a)) remote hoppings between the first and third layers have different strength and sign. We use $\gamma_2 = -0.02$ (same as ABC-stacked) and $\gamma_1 = 0.4, \gamma_5 = 0.04$ throughout this work [69]. The displacement field and superlattice potential are implemented by the same matrices as for ABC-stacked TLG, i.e., Eqs. (2) and (3). In the absence of remote hopping terms, the spectrum of ABA-stacked TLG consists of a linear and a quadratic crossing, shown in Fig. 8(b). However, unlike ABC-stacked TLG, in Bernal-stacked ABA TLG the external displacement field V_0 does not gap out the spectrum completely. Instead, the effect of V_0 is to gap the linear cone but leave the quadratic touching gapless. When the remote hopping terms are included, the spectrum becomes fully gapped; turning up V_0 further increases the gap of the linear cone, but does not change the overall band gap. As we will see, this has important consequences for the realization of the stacked band regime.

Fig. 9 shows the effect of a superlattice potential and displacement field on ABA-stacked TLG without (Fig. 9(a-d)) and with (Fig. 9(e-h)) the remote hopping terms. Starting with $V_0 = 0$ and a weak superlattice potential, including the remote hoppings causes two bands to completely detach from the rest of the bands, as shown in Fig. 9(f). Importantly, one of the detached bands is topological with Chern number $C = -1$. As V_{SL} is further turned up, topological flat bands with higher Chern numbers can also emerge, as shown in Fig. 9(g). However, even for a strong potential and non-zero displacement field the stacked flat band regime does not appear.

We hypothesize that the stacked flat band regime requires a large and tunable band gap in the $V_{SL} = 0$ limit; intuitively, the large band gap provides an energy window that can host bands detached by the superlattice potential. As explained below Eq. (8), V_0 does not change the low-energy band gap. Thus, to test our hypothesis, we introduce a tunable band gap via a sublattice mass m as follows:

$$H_m = m \begin{pmatrix} \sigma^z & \mathbf{0}_2 & \mathbf{0}_2 \\ \mathbf{0}_2 & \delta\sigma^z & \mathbf{0}_2 \\ \mathbf{0}_2 & \mathbf{0}_2 & \sigma^z \end{pmatrix}, \tag{9}$$

where σ^i are Pauli matrices of sublattice space. The mass m may result from TLG sandwiched between two layers of aligned hexagonal boron nitride, so that the middle layer feels only a ratio $0 \leq \delta < 1$ of mass m. Although this set-up would not result in a tunable value of m, we treat m as a tunable paramter to illustrate the vital effect of a tunable band gap. Fig. 10 shows that as m is turned up, the stacked flat band regime appears, even with $V_0 = 0$. However, compared to chiral TLG, the stack of flat bands does not span as wide an energy range as in chiral TLG.

In summary, the phenomenology of Bernal TLG differs from chiral stacking in two ways: first, unlike chiral stacked TLG, Bernal stacked TLG can easily realize topological flat bands in the weak field limit even for larger L. Second, the displacement field cannot induce the stacked flat band regime in Bernal stacked TLG; though the sublattice mass can play a similar role, it has less potency.

B. ABAB

We now discuss Bernal (ABAB-stacked) QLG, shown in Fig. 4(a), which is described by the following low-energy Hamiltonian,

$$H_{ABAB}(\mathbf{k}) = \begin{pmatrix} H_{\mathbf{G}} & \Gamma_1 & \Gamma_2 & \mathbf{0}_2 \\ \Gamma_1^\dagger & H_{\mathbf{G}} & \Gamma_1^\dagger & \Gamma_2' \\ \Gamma_2^\dagger & \Gamma_1 & H_{\mathbf{G}} & \Gamma_1 \\ \mathbf{0}_2 & \Gamma_2'^\dagger & \Gamma_1^\dagger & H_{\mathbf{G}} \end{pmatrix}, \tag{10}$$

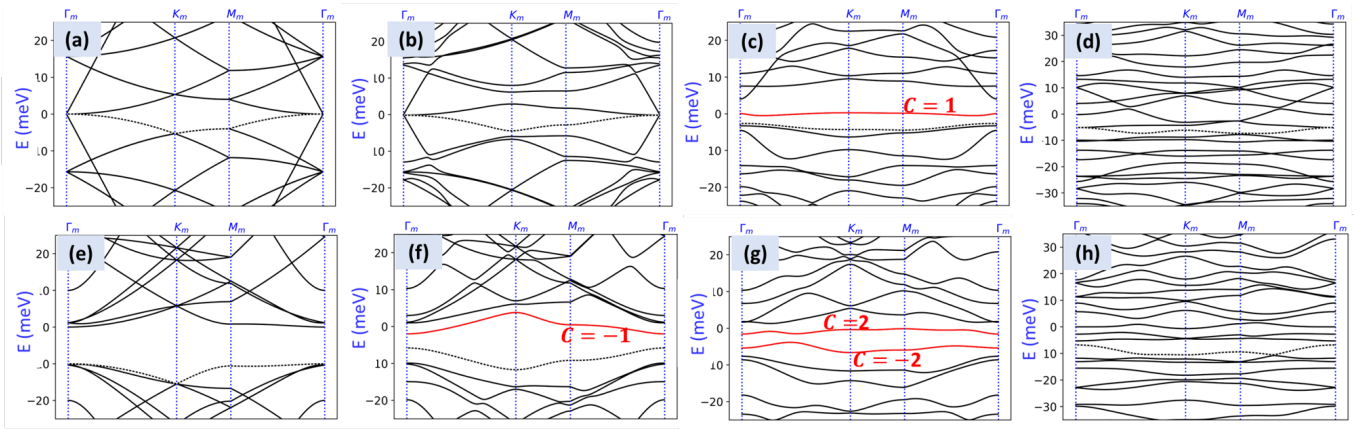

FIG. 9. Band structure of ABA-stacked TLG with a triangular superlattice potential in absence of sublattice mass $m = 0$ without (a-d) and with (e-h) remote hoppings. (a,e) $V_{SL} = 0$, $V_0 = 0$ meV, (b,f) $V_{SL} = 5$, $V_0 = 0$ meV, (c,g) $V_{SL} = 17$, $V_0 = 0$ meV, (d,h) $V_{SL} = 30$, $V_0 = -60$ meV

where

$$\Gamma_1 = \begin{pmatrix} 0 & v_3\pi \\ \gamma_1 & 0 \end{pmatrix}, \Gamma_2 = \begin{pmatrix} \gamma_2/2 & 0 \\ 0 & \gamma_5/2 \end{pmatrix}, \Gamma_2' = \begin{pmatrix} \gamma_5/2 & 0 \\ 0 & \gamma_2/2 \end{pmatrix} \tag{11}$$

The energy spectrum of Eq. (10) shows two pairs of quadratically dispersing bands in the absence of remote hoppings; see 4(c). Unlike Bernal TLG, the remote hopping terms do not gap the spectrum, but split the two quadratic nodes into three pairs of linear Dirac cones. A new feature is that one of the nodes in each pair has a small energy shift and tilt with respect to other nodes.

The band spectra in the presence of the superlattice potential are shown in Fig. 11. Fig. 11(d) shows the energy shift of the Dirac points when the remote hopping terms are included, as well as severe particle-hole symmetry breaking compared to (a). In general, topological flat bands do not appear without fine-tuning, although they can appear when remote hopping terms are included, as in Fig. 11(e). Increasing V_0 produces flatter bands both with and without the remote hopping terms, as shown in (c) and (f), although they are not isolated. Thus, the stacked flat band regime is more accessible than in Bernal TLG but less favorable compared to the chiral-stacked structures.

Though isolated flat bands are not readily available in Bernal QLG, topological bands (including those with $|C| > 1$) can be realized more generically when a sublattice mass term is included in addition to the displacement field, as shown in Fig. 12(a) for a smaller value of L. We incorporate the effect of a sublattice mass through the term

$$H_m = m \begin{pmatrix} \sigma^z & \mathbf{0}_2 & \mathbf{0}_2 & \mathbf{0}_2 \\ \mathbf{0}_2 & \delta_1\sigma^z & \mathbf{0}_2 & \mathbf{0}_2 \\ \mathbf{0}_2 & \mathbf{0}_2 & \delta_2\sigma^z & \mathbf{0}_2 \\ \mathbf{0}_2 & \mathbf{0}_2 & \mathbf{0}_2 & \sigma^z \end{pmatrix}, \tag{12}$$

and use $\delta_1 = \delta_2 = 0.3$ throughout. Additional band structures with smaller values of L are shown in Fig. 12.

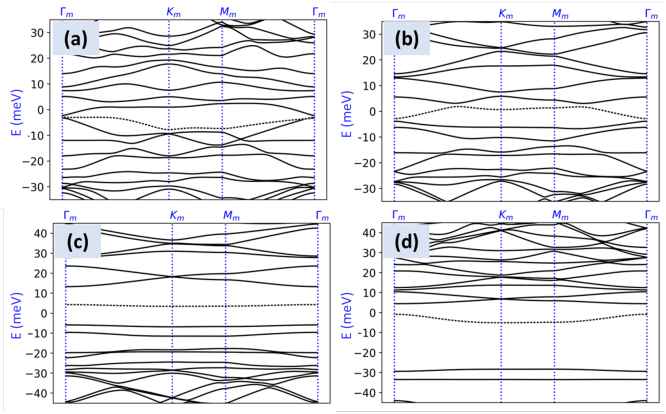

FIG. 10. Band structure of ABA-stacked TLG, varying the sublattice mass m at fixed gate potentials $V_{SL} = 20$, $V_0 = 0$ meV. (a-d) Spectrum with $m = 10$, 30, 50, -50 meV, respectively. Stacks of flat bands start to appear in (c) and (d). In all plots, remote hopping terms are included and $\delta = 0.3$.

IV. TWO SUPERLATTICE POTENTIALS

We briefly discuss the possibility of employing two superlattice potentials, one on the bottom and the other at the top of the sample. The motivation for considering such a setup is that the effect of the superlattice potential becomes vanishingly small for the upper layers of multilayer graphene.

To model this set-up, the parameters α, β, and η, which parameterize the superlattice potential in each layer relative to the first layer, as defined in Eqs. (3) and (7), must be modified. To reflect the symmetry of the set-up, we choose $\alpha = 0.5$, $\beta = 1$ in TLG and $\alpha = 0.3$, $\beta = 0.3$, and $\eta = 1$ in QLG.

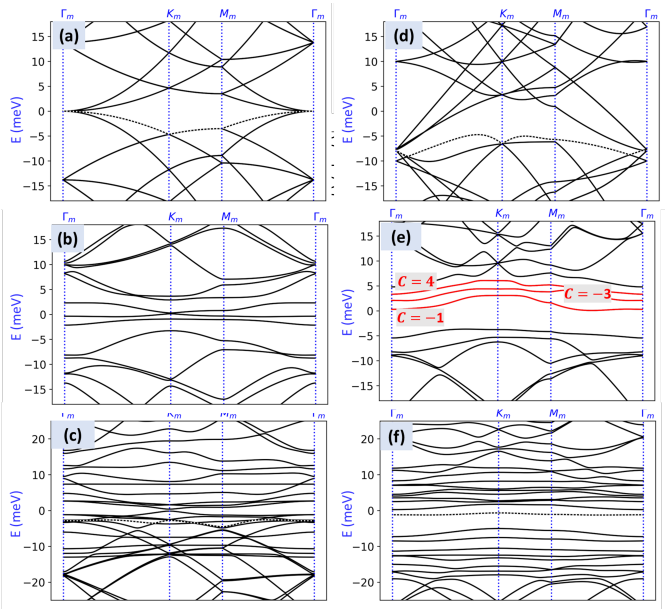

FIG. 11. Band structure of ABAB-stacked QLG with a superlattice potential, without (a-c) and with (d-f) the remote hoppings; (a,d) $V_{SL} = 0$, $V_0 = 0$ meV, (b,e) $V_{SL} = 10$, $V_0 = 30$ meV, (c,f) $V_{SL} = 20$, $V_0 = -100$ meV. For smaller potentials, topological flat bands can be realized when the remote hopping terms are included, although they are not isolated and require fine-tuning. For larger potentials, flat bands appear with and without remote hopping terms, as in (c) and (f), though they are not isolated.

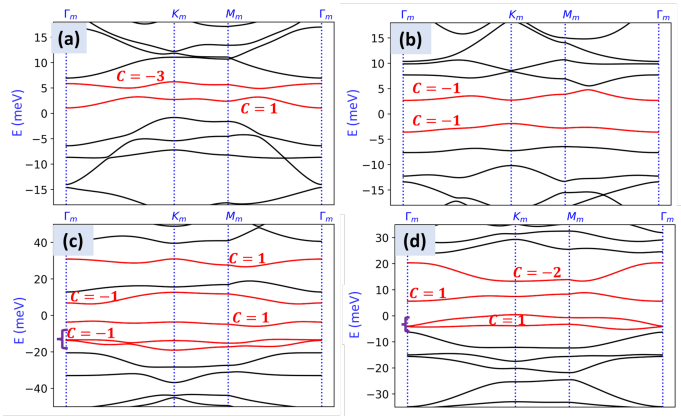

FIG. 12. Two superlattice potentials realize topological flat bands (red) in multilayer graphene. (a) Bernal QLG with a single superlattice potential with $V_{SL} = 40$, $V_0 = 60$, $m = 20$ meV, $L = 40$ nm, $\alpha = 0.3$, $\beta = 0.1$, $\eta = 0$, and $\delta_1 = \delta_2 = 0.3$; (b) Bernal QLG with two superlattice potentials, $V_{SL} = 20$, $V_0 = 50$, $m = 20$ meV, $L = 40$ nm, $\alpha = 0.3$, $\beta = 0.3$, $\eta = 1$, and $\delta_1 = \delta_2 = 0.3$; (c) chiral QLG with with two superlattice potentials, $V_{SL} = 25$, $V_0 = 20$ meV, $L = 25$ nm and $\alpha = 0.3$, $\beta = 0.3$, $\eta = 1$; (d) chiral TLG with with two superlattice potential $V_{SL} = 30$, $V_0 = 30$ meV, $L = 35$ nm and $\alpha = 0.5$, $\beta = 1$. Parameters are chosen to minimize the bandwidth of topological bands.

In Fig. 12(b), we show the effect of two superlattice potentials on Bernal-stacked QLG. We find that the two superlattice setup is capable of generating flatter topological bands even for weaker fields compared to the single superlattice potential setup (Fig. 12(a)) because more layers feel the potential.

In the chiral-stacked case with two potentials, new phenomena appear. As shown in Fig. 12(c,d), for both chiral TLG and QLG, multiple topological bands with small bandwidth can appear, including those with $|C| > 1$; the parameters in each figure are chosen to produce the flattest topological bands. In contrast, topological flat bands never occurred in the single potential setups for TLG and QLG with large L as shown in Figs. 3 and 5. We conclude that the two superlattice potential setup may offer advantages over a single superlattice potential in realizing topological flat bands.

V. CONCLUDING REMARKS AND PRACTICAL RECIPES FOR EXPERIMENT

We performed a comprehensive study of flat bands in multilayer graphene subject to a superlattice potential. In [59] we showed that a superlattice potential induces two distinct regimes of flat bands in bilayer graphene, namely topological and stacked flat bands. In this work, we discussed the realization of these phases in graphene structures with more layers, which can be either chirally or Bernal stacked. Our conclusions provide a cookbook for experimental realizations of flat bands in multilayer graphene structures with a superlattice potential.

Our main conclusions are as follows: (1) Chirally stacked graphene multilayers are ideal to realize the stacked flat band regime. The higher the number of layers, the easier it is to get to that regime. However, topological bands can be achieved for smaller values of L. (2) Bernal stacked graphene is favorable for realizing topological flat bands in setups with a single superlattice potential. It does not realize the stacked flat band regime and becomes worse by increasing the number of layers. (3) A sublattice mass (e.g., provided by hBN) can induce a gap in Bernal stacked multilayers, which can help generate stacked flat bands. However, we do not have a physical system in mind where such a mass is tunable. Artificial metamaterials may be helpful to realize this tunable mass. (4) The remote hoppings impact the realization of isolated flat bands in multilayer graphene at small fields and become more relevant as the number of layers increases. (5) Due to the increased low-energy density of states as the number of layers increases, a smaller superlattice period is imperative to obtain isolated flat bands. (6) Using two superlattice potentials enhances the effect of the superlattice and may be promising to achieve both the topological and stacked flat bands in chirally stacked multilayer graphene.

Our results demonstrate the generality and robustness of both the topological and stacked regimes of flat

bands in multilayer graphene with an artificial superlattice potential. Thus, these systems provide a promising platform for quantum simulation and an alternative to twisted heterostructures. Future theoretical and experimental studies will demonstrate the correlated phenomena that derive from both flat band regimes.

ACKNOWLEDGEMENTS

The authors acknowledge a useful conversation with Senthil Todadri. This work was supported by the Air Force Office of Scientific Research under Grant No. FA9550-20-1-0260. J.C. is partially supported by the Alfred P. Sloan Foundation through a Sloan Research Fellowship. The Flatiron Institute is a division of the Simons Foundation.

[1] R. Bistritzer and A. H. MacDonald, Moiré bands in twisted double-layer graphene, Proceedings of the National Academy of Sciences **108**, 12233 (2011).
[2] Y. Cao, V. Fatemi, S. Fang, K. Watanabe, T. Taniguchi, E. Kaxiras, and P. Jarillo-Herrero, Unconventional superconductivity in magic-angle graphene superlattices, Nature **556**, 43 (2018).
[3] M. Yankowitz, S. Chen, H. Polshyn, Y. Zhang, K. Watanabe, T. Taniguchi, D. Graf, A. F. Young, and C. R. Dean, Tuning superconductivity in twisted bilayer graphene, Science **363**, 1059 (2019).
[4] X. Lu, P. Stepanov, W. Yang, M. Xie, M. A. Aamir, I. Das, C. Urgell, K. Watanabe, T. Taniguchi, G. Zhang, A. Bachtold, A. H. MacDonald, and D. K. Efetov, Superconductors, orbital magnets and correlated states in magic-angle bilayer graphene, Nature **574**, 653 (2019).
[5] M. Serlin, C. Tschirhart, H. Polshyn, Y. Zhang, J. Zhu, K. Watanabe, T. Taniguchi, L. Balents, and A. Young, Intrinsic quantized anomalous hall effect in a moiré heterostructure, Science **367**, 900 (2020).
[6] K. P. Nuckolls, M. Oh, D. Wong, B. Lian, K. Watanabe, T. Taniguchi, B. A. Bernevig, and A. Yazdani, Strongly correlated chern insulators in magic-angle twisted bilayer graphene, Nature **588**, 610 (2020).
[7] G. Chen, A. L. Sharpe, E. J. Fox, Y.-H. Zhang, S. Wang, L. Jiang, B. Lyu, H. Li, K. Watanabe, T. Taniguchi, Z. Shi, T. Senthil, D. Goldhaber-Gordon, Y. Zhang, and F. Wang, Tunable correlated Chern insulator and ferromagnetism in a moiré superlattice, Nature **579**, 56 (2020).
[8] Y. Xie, A. T. Pierce, J. M. Park, D. E. Parker, E. Khalaf, P. Ledwith, Y. Cao, S. H. Lee, S. Chen, P. R. Forrester, K. Watanabe, T. Taniguchi, A. Vishwanath, P. Jarillo-Herrero, and A. Yacoby, Fractional chern insulators in magic-angle twisted bilayer graphene, Nature **600**, 439 (2021).
[9] Y. Cao, V. Fatemi, A. Demir, S. Fang, S. L. Tomarken, J. Y. Luo, J. D. Sanchez-Yamagishi, K. Watanabe, T. Taniguchi, E. Kaxiras, R. C. Ashoori, and P. Jarillo-Herrero, Correlated insulator behaviour at half-filling in magic-angle graphene superlattices, Nature **556**, 80 (2018).
[10] Y. Xu, S. Liu, D. A. Rhodes, K. Watanabe, T. Taniguchi, J. Hone, V. Elser, K. F. Mak, and J. Shan, Correlated insulating states at fractional fillings of moiré superlattices, Nature **587**, 214 (2020).
[11] J. Wang, Y. Zheng, A. J. Millis, and J. Cano, Chiral approximation to twisted bilayer graphene: Exact intravalley inversion symmetry, nodal structure, and implications for higher magic angles, Physical Review Research **3**, 023155 (2021).
[12] Y. Tang, L. Li, T. Li, Y. Xu, S. Liu, K. Barmak, K. Watanabe, T. Taniguchi, A. H. MacDonald, J. Shan, and K. F. Mak, Simulation of hubbard model physics in wse2/ws2 moiré superlattices, Nature **579**, 353 (2020).
[13] E. C. Regan, D. Wang, C. Jin, M. I. B. Utama, B. Gao, X. Wei, S. Zhao, W. Zhao, Z. Zhang, K. Yumigeta, M. Blei, J. D. Carlström, K. Watanabe, T. Taniguchi, S. Tongay, M. Crommie, A. Zettl, and F. Wang, Mott and generalized Wigner crystal states in WSe_2/WS_2 moiré superlattices, Nature **579**, 359 (2020).
[14] D. M. Kennes, M. Claassen, L. Xian, A. Georges, A. J. Millis, J. Hone, C. R. Dean, D. N. Basov, A. N. Pasupathy, and A. Rubio, Moiré heterostructures as a condensed-matter quantum simulator, Nature Physics 2021 17:2 **17**, 155 (2021).
[15] X. Liu, Z. Hao, E. Khalaf, J. Y. Lee, Y. Ronen, H. Yoo, D. H. Najafabadi, K. Watanabe, T. Taniguchi, A. Vishwanath, and P. Kim, Tunable spin-polarized correlated states in twisted double bilayer graphene, Nature **583**, 221 (2020).
[16] M. He, Y. Li, J. Cai, Y. Liu, K. Watanabe, T. Taniguchi, X. Xu, and M. Yankowitz, Symmetry breaking in twisted double bilayer graphene, Nature Physics **17**, 26 (2021).
[17] G. W. Burg, J. Zhu, T. Taniguchi, K. Watanabe, A. H. MacDonald, and E. Tutuc, Correlated insulating states in twisted double bilayer graphene, Phys. Rev. Lett. **123**, 197702 (2019).
[18] C. Shen, Y. Chu, Q. Wu, N. Li, S. Wang, Y. Zhao, J. Tang, J. Liu, J. Tian, K. Watanabe, R. Yang, Z. Y. Meng, D. Shi, O. V. Yazyev, and G. Zhang, Correlated states in twisted double bilayer graphene, Nature Physics **16**, 520 (2020).
[19] Y. Cao, D. Rodan-Legrain, O. Rubies-Bigorda, J. M. Park, K. Watanabe, T. Taniguchi, and P. Jarillo-Herrero, Tunable correlated states and spin-polarized phases in twisted bilayer-bilayer graphene, Nature **583**, 215 (2020).
[20] J. M. Park, Y. Cao, K. Watanabe, T. Taniguchi, and P. Jarillo-Herrero, Tunable strongly coupled superconductivity in magic-angle twisted trilayer graphene, Nature **590**, 249 (2021).
[21] S. Xu, M. M. A. Ezzi, N. Balakrishnan, A. Garcia-Ruiz, B. Tsim, C. Mullan, J. Barrier, N. Xin, B. A. Piot, T. Taniguchi, K. Watanabe, A. Carvalho, A. Mishchenko, A. K. Geim, V. I. Fal'ko, S. Adam, A. H. C. Neto, K. S. Novoselov, and Y. Shi, Tunable van hove singularities and correlated states in twisted monolayer–bilayer graphene, Nature Physics **17**, 619 (2021).

[22] S. Chen, M. He, Y.-H. Zhang, V. Hsieh, Z. Fei, K. Watanabe, T. Taniguchi, D. H. Cobden, X. Xu, C. R. Dean, and M. Yankowitz, Electrically tunable correlated and topological states in twisted monolayer-bilayer graphene, Nature Physics **17**, 374 (2021).

[23] Z. Hao, A. Zimmerman, P. Ledwith, E. Khalaf, D. H. Najafabadi, K. Watanabe, T. Taniguchi, A. Vishwanath, and P. Kim, Electric field–tunable superconductivity in alternating-twist magic-angle trilayer graphene, Science **371**, 1133 (2021).

[24] J. M. Park, Y. Cao, L. Xia, S. Sun, K. Watanabe, T. Taniguchi, and P. Jarillo-Herrero, Magic-angle multilayer graphene: A robust family of moiré superconductors, arXiv preprint arXiv:2112.10760 (2021).

[25] F. Wu, T. Lovorn, E. Tutuc, I. Martin, and A. H. MacDonald, Topological insulators in twisted transition metal dichalcogenide homobilayers, Phys. Rev. Lett. **122**, 086402 (2019).

[26] L. Wang, E.-M. Shih, A. Ghiotto, L. Xian, D. A. Rhodes, C. Tan, M. Claassen, D. M. Kennes, Y. Bai, B. Kim, K. Watanabe, T. Taniguchi, X. Zhu, J. Hone, A. Rubio, A. N. Pasupathy, and C. R. Dean, Correlated electronic phases in twisted bilayer transition metal dichalcogenides, Nature materials **19**, 861 (2020).

[27] F. Wu, T. Lovorn, E. Tutuc, and A. H. MacDonald, Hubbard model physics in transition metal dichalcogenide moiré bands, Phys. Rev. Lett. **121**, 026402 (2018).

[28] T. Devakul, V. Crépel, Y. Zhang, and L. Fu, Magic in twisted transition metal dichalcogenide bilayers, Nature communications **12**, 1 (2021).

[29] J. Zang, J. Wang, J. Cano, and A. J. Millis, Hartree-fock study of the moiré hubbard model for twisted bilayer transition metal dichalcogenides, Phys. Rev. B **104**, 075150 (2021).

[30] Z. Bi and L. Fu, Excitonic density wave and spin-valley superfluid in bilayer transition metal dichalcogenide, Nature communications **12**, 1 (2021).

[31] J. Wang, J. Zang, J. Cano, and A. J. Millis, Staggered pseudo magnetic field in twisted transition metal dichalcogenides: Physical origin and experimental consequences, arXiv preprint arXiv:2110.14570 (2021).

[32] J. Zang, J. Wang, J. Cano, A. Georges, and A. J. Millis, Dynamical mean field theory of moiré bilayer transition metal dichalcogenides: phase diagram, resistivity, and quantum criticality, arXiv preprint arXiv:2112.03080 (2021).

[33] A. Wietek, J. Wang, J. Zang, J. Cano, A. Georges, and A. Millis, Tunable stripe order and weak superconductivity in the moir\'e hubbard model, arXiv preprint arXiv:2204.04229 (2022).

[34] L. Xian, M. Claassen, D. Kiese, M. M. Scherer, S. Trebst, D. M. Kennes, and A. Rubio, Realization of nearly dispersionless bands with strong orbital anisotropy from destructive interference in twisted bilayer MoS_2, Nature Communications **12**, 5644 (2021), arXiv:2004.02964 [cond-mat.mes-hall].

[35] L. Klebl, Q. Xu, A. Fischer, L. Xian, M. Claassen, A. Rubio, and D. M. Kennes, Moiré engineering of spin-orbit coupling in twisted platinum diselenide, Electronic Structure **4**, 014004 (2022).

[36] K. Hejazi, Z.-X. Luo, and L. Balents, Noncollinear phases in moiré magnets, Proceedings of the National Academy of Sciences **117**, 10721 (2020).

[37] Y. Xu, A. Ray, Y.-T. Shao, S. Jiang, D. Weber, J. E. Goldberger, K. Watanabe, T. Taniguchi, D. A. Muller, K. F. Mak, and J. Shan, Emergence of a noncollinear magnetic state in twisted bilayer CrI_3 10.48550/ARXIV.2103.09850 (2021).

[38] T. Song, Q.-C. Sun, E. Anderson, C. Wang, J. Qian, T. Taniguchi, K. Watanabe, M. A. McGuire, R. Stöhr, D. Xiao, T. Cao, J. Wrachtrup, and X. Xu, Direct visualization of magnetic domains and moiré magnetism in twisted 2d magnets, Science **374**, 1140 (2021).

[39] P. A. Volkov, J. H. Wilson, and J. Pixley, Magic angles and current-induced topology in twisted nodal superconductors, arXiv preprint arXiv:2012.07860 (2020).

[40] O. Can, T. Tummuru, R. P. Day, I. Elfimov, A. Damascelli, and M. Franz, High-temperature topological superconductivity in twisted double-layer copper oxides, Nature Physics **17**, 519 (2021).

[41] S. Y. F. Zhao, N. Poccia, X. Cui, P. A. Volkov, H. Yoo, R. Engelke, Y. Ronen, R. Zhong, G. Gu, S. Plugge, T. Tummuru, M. Franz, J. H. Pixley, and P. Kim, Emergent interfacial superconductivity between twisted cuprate superconductors, arXiv preprint arXiv:2108.13455 (2021).

[42] A. Dunbrack and J. Cano, Magic angle conditions for twisted 3d topological insulators, arXiv preprint arXiv:2112.11464 10.48550/ARXIV.2112.11464 (2021).

[43] D. Guerci, J. Wang, J. Zang, J. Cano, J. Pixley, and A. Millis, Chiral kondo lattice in doped $MoTe_2WSe_2$ bilayers, arXiv preprint arXiv:2207.06476 (2022).

[44] C. N. Lau, M. W. Bockrath, K. F. Mak, and F. Zhang, Reproducibility in the fabrication and physics of moiré materials, Nature **602**, 41 (2022).

[45] C. Forsythe, X. Zhou, K. Watanabe, T. Taniguchi, A. Pasupathy, P. Moon, M. Koshino, P. Kim, and C. R. Dean, Band structure engineering of 2d materials using patterned dielectric superlattices, Nature nanotechnology **13**, 566 (2018).

[46] Y. Li, S. Dietrich, C. Forsythe, T. Taniguchi, K. Watanabe, P. Moon, and C. R. Dean, Anisotropic band flattening in graphene with one-dimensional superlattices, Nature Nanotechnology **16**, 525 (2021).

[47] D. Barcons Ruiz, H. Herzig Sheinfux, R. Hoffmann, I. Torre, H. Agarwal, R. K. Kumar, L. Vistoli, T. Taniguchi, K. Watanabe, A. Bachtold, and F. H. L. Koppens, Engineering high quality graphene superlattices via ion milled ultra-thin etching masks, Nature Communications **13**, 1 (2022).

[48] C.-H. Park, L. Yang, Y.-W. Son, M. L. Cohen, and S. G. Louie, Anisotropic behaviours of massless dirac fermions in graphene under periodic potentials, Nature Physics **4**, 213 (2008).

[49] C.-H. Park, L. Yang, Y.-W. Son, M. L. Cohen, and S. G. Louie, New generation of massless dirac fermions in graphene under external periodic potentials, Phys. Rev. Lett. **101**, 126804 (2008).

[50] C.-H. Park and S. G. Louie, Making massless dirac fermions from a patterned two-dimensional electron gas, Nano letters **9**, 1793 (2009).

[51] M. Barbier, P. Vasilopoulos, and F. M. Peeters, Extra dirac points in the energy spectrum for superlattices on single-layer graphene, Phys. Rev. B **81**, 075438 (2010).

[52] S. Dubey, V. Singh, A. K. Bhat, P. Parikh, S. Grover, R. Sensarma, V. Tripathi, K. Sengupta, and M. M. Deshmukh, Tunable superlattice in graphene to control the

number of dirac points, Nano letters **13**, 3990 (2013).
[53] L. A. Ponomarenko, R. V. Gorbachev, G. L. Yu, D. C. Elias, R. Jalil, A. A. Patel, A. Mishchenko, A. S. Mayorov, C. R. Woods, J. R. Wallbank, M. Mucha-Kruczynski, B. A. Piot, M. Potemski, I. V. Grigorieva, K. S. Novoselov, F. Guinea, V. I. Fal'ko, and A. K. Geim, Cloning of dirac fermions in graphene superlattices, Nature **497**, 594 (2013).
[54] R. Huber, M.-H. Liu, S.-C. Chen, M. Drienovsky, A. Sandner, K. Watanabe, T. Taniguchi, K. Richter, D. Weiss, and J. Eroms, Gate-tunable two-dimensional superlattices in graphene, Nano letters **20**, 8046 (2020).
[55] X. Lu, S. Zhang, Z. V. Han, and J. Liu, Synergistic interplay between dirac fermions and long-wavelength order parameters in graphene-insulator heterostructures 10.48550/ARXIV.2206.05659 (2022).
[56] M. Killi, S. Wu, and A. Paramekanti, Band structures of bilayer graphene superlattices, Phys. Rev. Lett. **107**, 086801 (2011).
[57] S. Wu, M. Killi, and A. Paramekanti, Graphene under spatially varying external potentials: Landau levels, magnetotransport, and topological modes, Phys. Rev. B **85**, 195404 (2012).
[58] A. Ramires and J. L. Lado, Electrically tunable gauge fields in tiny-angle twisted bilayer graphene, Phys. Rev. Lett. **121**, 146801 (2018).
[59] S. A. A. Ghorashi, A. Dunbrack, J. Sun, X. Du, and J. Cano, Topological and stacked flat bands in bilayer graphene with a superlattice potential 10.48550/ARXIV.2206.13501 (2022).
[60] J. Cano, S. Fang, J. H. Pixley, and J. H. Wilson, Moiré superlattice on the surface of a topological insulator, Phys. Rev. B **103**, 155157 (2021).
[61] T. Wang, N. F. Q. Yuan, and L. Fu, Moiré surface states and enhanced superconductivity in topological insulators, Phys. Rev. X **11**, 021024 (2021).
[62] D. Guerci, J. Wang, J. H. Pixley, and J. Cano, Designer meron lattice on the surface of a topological insulator 10.48550/ARXIV.2203.04986 (2022).
[63] L.-k. Shi, J. Ma, and J. C. Song, Gate-tunable flat bands in van der waals patterned dielectric superlattices, 2D Materials **7**, 015028 (2019).
[64] H. Min and A. H. MacDonald, Electronic structure of multilayer graphene, Progress of Theoretical Physics Supplement **176**, 227 (2008).
[65] F. Zhang, B. Sahu, H. Min, and A. H. MacDonald, Band structure of *abc*-stacked graphene trilayers, Phys. Rev. B **82**, 035409 (2010).
[66] H. Rokni and W. Lu, Layer-by-layer insight into electrostatic charge distribution of few-layer graphene, Scientific reports **7**, 1 (2017).
[67] Y.-H. Zhang, D. Mao, Y. Cao, P. Jarillo-Herrero, and T. Senthil, Nearly flat chern bands in moiré superlattices, Phys. Rev. B **99**, 075127 (2019).
[68] G. Chen, L. Jiang, S. Wu, B. Lyu, H. Li, B. L. Chittari, K. Watanabe, T. Taniguchi, Z. Shi, J. Jung, *et al.*, Evidence of a gate-tunable mott insulator in a trilayer graphene moiré superlattice, Nature Physics **15**, 237 (2019).
[69] A. A. Zibrov, P. Rao, C. Kometter, E. M. Spanton, J. I. A. Li, C. R. Dean, T. Taniguchi, K. Watanabe, M. Serbyn, and A. F. Young, Emergent dirac gullies and gully-symmetry-breaking quantum hall states in *aba* trilayer graphene, Phys. Rev. Lett. **121**, 167601 (2018).